Chinese Chemical Letters 34 (2023) 107899

Contents lists available at ScienceDirect

Chinese Chemical Letters

journal homepage: www.elsevier.com/locate/cclet

A new insight into the promoting effects of transition metal phosphides in methanol electrooxidation

Junjie Ding[a,1], Shaojie Jing[a,1], Changqing Yin[b], Chaogang Ban[a], Kaiwen Wang[c], Xue Liu[a], Youyu Duan[a], Yuxin Zhang[b], Guang Han[b], Liyong Gan[a,*], Jinsong Rao[b,*]

[a] College of Physics and Center of Quantum Materials and Devices, Chongqing University, Chongqing 401331, China
[b] College of Material Science and Engineering, Chongqing University, Chongqing 400044, China
[c] Beijing Key Laboratory of Microstructure and Property of Advanced Materials, Beijing University of Technology, Beijing 100024, China

ARTICLE INFO

Article history:
Received 31 July 2022
Revised 11 August 2022
Accepted 11 October 2022
Available online 17 October 2022

Keywords:
Promoting effect
Transition metal phosphides
Pt-Co-P composite
Catalytic mechanisms
Methanol oxidation reaction

ABSTRACT

The construction of highly active catalysts for methanol oxidation reaction (MOR) is central to direct methanol fuel cells. Tremendous progress has been made in transition metal phosphides (TMPs) based catalysts. However, TMPs would be partially damaged and transformed into new substances (*e.g.*, Pt-M-P composite, where M represents a second transition metal) during Pt deposition process. This would pose a large obstacle to the cognition of the real promoting effects of TMPs in MOR. Herein, Co_2P co-catalysts (Pt-P/Co_2P@NPC, where NPC stands for N and P co-doped carbon) and Pt-Co-P composite catalysts (Pt-Co-P/NPC) were controllably synthesized. Electrocatalysis tests show that the Pt-Co-P/NPC exhibits superior MOR activity as high as 1016 mA/mg_{Pt}, significantly exceeding that of Pt-P/Co_2P@NPC (345 mA/mg_{Pt}). This result indicates that the promoting effect is ascribed primarily to the resultant Pt-Co-P composite, in sharply contrast to previous viewpoint that Co_2P itself improves the activity. Further mechanistic studies reveal that Pt-Co-P/NPC exhibits much stronger electron interaction and thus manifesting a remarkably weaker CO absorption than Pt-P/Co_2P@NPC and Pt/C. Moreover, Pt-Co-P is also more capable of producing oxygen-containing adsorbate and thus accelerating the removal of surface-bonded CO*, ultimately boosting the MOR performance.

Advanced clean energy technologies, such as solar cells and fuel cells, are expected to play a crucial role in energy conversion and storage in the future due to their environmental friendliness and sustainability [1–3]. In recent years, direct methanol fuel cells (DMFCs) receive intensive attention due to their abundant fuel sources, high conversion efficiency as well as low pollutant emission [4–6]. However, its commercial success is seriously obstructed by the low activity of anode methanol oxidation reaction (MOR) catalysts to a large extent [7]. To date, expensive Pt-based catalysts are irreplaceable in DMFCs because almost all Pt-free catalysts exhibit negligible MOR activity in acidic medium. What's worse, Pt-based MOR catalysts are highly prone to be poisoned by CO that is generated from the dehydrogenation of methanol molecules, degrading the activity and durability [8,9]. Despite tremendous progress has been made in MOR catalysts, such as some bimetallic alloys [10], most synthetic methods usually involved expensive and toxic precursors [2,11], severely hindering their large-scale commercialization. Accordingly, developing highly active and alternative MOR catalysts is central to wide penetration of DMFCs [4,12].

To design excellent MOR catalysts, another strategy, *i.e.*, introducing co-catalysts, has been investigated, such as transition metal oxides, hydroxides, carbides, nitrides, and phosphides [13–20]. Among the above listed co-catalysts, transition metal phosphides (TMPs) stand out due to their relatively high electrical conductivity [21]. For example, Xing's group reported a significantly improved MOR activity by using Ni_2P and CoP as co-catalysts. Chang *et al.* found that bimetallic phosphides had overwhelming advantages over single TMPs counterparts in MOR [20,22–24]. Moreover, these outstanding progresses have led to a bi-functional mechanism and an electronic mechanism that rationalize the promoting effects of TMP co-catalysts. The former asserts that TMPs can catalyze water dissociation at a lower potential (< 0.7 V *vs.* reversible hydrogen electrode) due to the existence of positive metal center ($M^{\delta+}$) and negative $P^{\delta-}$ active sites [21]. As a result, affluent oxygen-containing adsorbates (OH*) are generated, facilitating the elimination of surface-bonded CO* [10,25]. The latter claims that

* Corresponding authors.
E-mail addresses: ganly@cqu.edu.cn (L. Gan), rjs@cqu.edu.cn (J. Rao).
[1] These authors contributed equally to this work.

https://doi.org/10.1016/j.cclet.2022.107899
1001-8417/

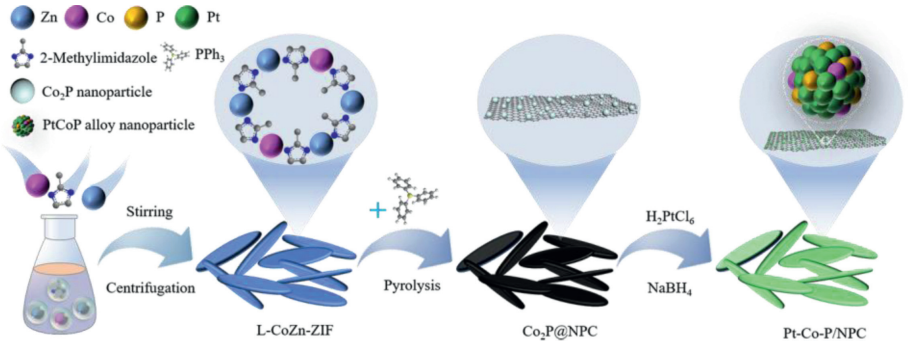

Scheme 1. Schematic illustration of the fabrication process of Pt-Co-P/NPC.

TMPs induces an electronic effect that lowers the D-band center of Pt, and thus weakens the adsorption strength of CO* [25].

Different from non-supported catalysts (*e.g.,* some hydrogen evolution catalysts in which TMPs act as active sites), Pt deposition is inevitable for MOR, chloroplatinic acid (H_2PtCl_6) is usually the Pt source and additional reducing reagents are required [11,20]. In other words, the TMPs must endure the acidic and reductive environments. Otherwise, TMPs may be transformed into other species. A careful inspection of many pioneers' reports revealed that the morphology and structures of TMPs changed dramatically after Pt deposition [11,24]. Specifically, the X-ray diffraction peaks were remarkably weakened, indicating that the structures of TMPs were at least partially destructed. Besides, element mapping reflected that Pt, transition metals and P exhibited a synchronous distribution. These results clearly manifested the formation of new substance [11,26]. Therefore, the questions arise: What is the active species that catalyzes MOR when TMPs are applied?

In this work, we aim at ascertaining the promoting effect and especially identifying the real active species of TMPs in MOR, selecting the widely used Co_2P as a prototypic paradigm. Controlled experiments were conducted to achieve both well-preserved Co_2P co-catalyst (Pt-P/Co_2P@NPC) and *in-situ* formed Pt-Co-P composite catalyst (Pt-Co-P/NPC) from Co_2P/NPC. The comparison between the two catalysts provides an ideal platform to explore the authentic promoting effect of TMPs in MOR due to their similar fabrication processes, identical specific surface area and graphitic degree. Electrocatalysis tests show that Pt-Co-P/NPC exhibits a significantly higher MOR performance than Pt-P/Co_2P@NPC. The results clearly indicate that the promoting effect of Co_2P is ascribed primarily to the resultant Pt-Co-P composite rather than Co_2P itself. This finding is in sharp contrast to previous studies, which claimed that TMPs themselves play the dominant role in promoting MOR performance. In addition, further designed experiments and density functional theory (DFT) calculations reveal that the electron interactions and bi-functional effect are enhanced in Pt-Co-P. Therefore, the composite exhibits superior CO tolerance ability and ultimately higher MOR activity.

The target Pt-based catalysts were fabricated through three simple steps (Scheme 1). Initially, two types of leaf-like ZIF precursors (Fig. S1 in Supporting information) were obtained *via* an organic solvent-free method, followed by a synchronous phosphorization-pyrolysis procedure, the catalyst supports (Co_2P@NPC and NPC) can be yielded. The Co_2P@NPC exhibits a carbon framework morphology, embedded with crowds of visible particles (Fig. S2a in Supporting information), while the NPC exhibits a particle-free porous structure (Fig. S2b in Supporting information). Transmission electron microscopy (TEM) images (Figs. 1a and b) and elements mapping results (Fig. 1c) confirm that the Co_2P particles, with a mean size of *ca.* 40 nm, were formed and enclosed in NPC. The X-ray diffraction (XRD) results (Fig. S3a in

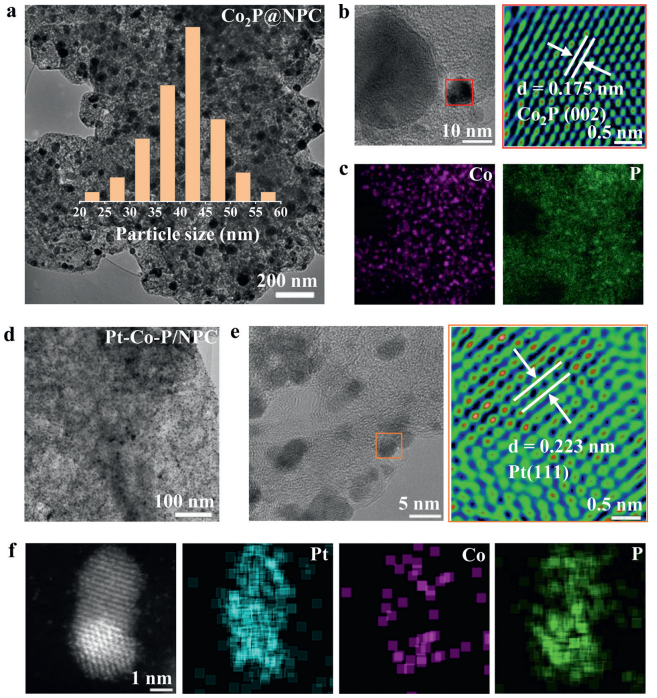

Fig. 1. (a) TEM, (b) HR-TEM image and (c) element mapping of Co and P for Co_2P@NPC. Inset in (a) shows the particle size distribution of Co_2P. (d) TEM, (e) HR-TEM image and (f) element mapping of Pt, Co and P for Pt-Co-P@NPC.

Supporting information) indicate that the formed Co_2P particles can be assigned to the orthorhombic phase [27]. Moreover, the energy dispersive X-ray (EDX) spectroscopy (Fig. S4 in Supporting information) shows that the Zn species are removed from the supports after thermal treatment.

The specific surface area is a vital structural parameter for the follow-up Pt deposition process. Both Co_2P@NPC and NPC exhibit a typical type IV isotherm (Figs. S5a and b in Supporting information). There are obvious tails in the low pressure and noteworthy hysteresis loops in the middle pressure region, manifesting their hierarchical porous structure [28,29]. The Co_2P@NPC shows a large Brunauer-Emmett-Teller specific surface area of 327.88 m^2/g, which is comparable to that of NPC (344.38 m^2/g). Raman spectra (Fig. S5c in Supporting information) reveal no significant difference in the intensity ratio of D and G band (denoted as I_D/I_G) of Co_2P@NPC (1.05) and NPC (1.06), indicating that the two supports have nearly identical graphitic degree and therefore comparable charge transfer resistance [30,31]. Therefore, the influences of specific surface area and electrical conductivity are expected to play a minor role in the differences of the electrocatalytic performance and thus can be safely ruled out [32].

In Pt deposition process, controlled experiments were conducted to prepare Pt-Co-P/NPC, Pt-P/NPC and Pt-P/Co_2P@NPC catalysts. Specifically, H_2PtCl_6 and K_2PtCl_6 were used as different Pt sources to produce the former two and the latter catalysts, respectively. Clearly, the characteristic diffraction peaks of face-centered cubic Pt emerge in the XRD patterns of the three catalysts (Fig. S3c in Supporting information) [33]. Besides, the synthesis of Pt-Co-P/NPC was accompanied by the apparent disappearance of Co_2P nanoparticles (Fig. 1d and Fig. S6a in Supporting information) due to the acidic condition. This is also confirmed by the XRD pattern of Pt-Co-P/NPC, where the diffraction peaks of Co_2P are completely disappeared (Fig. S3c). The morphology of Pt-P/Co_2P@NPC and Pt-P/NPC was almost unchanged after Pt deposition (Figs. S6b and c in Supporting information). The diffraction peaks of Co_2P are well preserved in Pt-P/Co_2P@NPC (Fig. S3c). The above results demonstrate that the controlled synthesis using different Pt sources not only successfully prepared Pt-based catalysts but also achieved preservation or disappearance of Co_2P.

High-resolution TEM (HR-TEM) images (Fig. 1e) of Pt-Co-P@NPC reveal a lattice spacing of 0.223 nm, which can be well indexed to the (111) plane of face-centered cubic Pt [33]. Meanwhile, the element distribution mapping (Fig. 1f) and EDX results (Fig. S7 in Supporting information) demonstrate that Pt, Co and P exhibit an analogous distribution feature, indicating the loading of Pt-Co-P composite on the surface of NPC rather than pure Pt [34]. Similarly, the Pt-P composite nanoparticles are also observed in Pt-P/Co_2P@NPC and Pt-P/NPC (Figs. S8 and S9 in Supporting information). The formation of Pt-Co-P can be attributed to the fact that Co and P were leached from Co_2P in the acidic environment and then co-reduced with Pt [35]. In contrast, Pt-P/Co_2P@NPC was synthesized in the non-acid solution, and Co_2P nanoparticles were well preserved. Meanwhile, the formation mechanism of Pt-P composite can be interpreted as soluble P was leached from the carbon frameworks and subsequently co-reduced with Pt. On the basis of above results, it is reasonable to deduce that the formation of Pt-based composite is inevitable under similar acidic conditions adopted by previous reports [11,24].

The MOR performances over the synthesized catalysts were comparatively investigated by cyclic voltammetry (CV) in 0.5 mol/L H_2SO_4 + 1 mol/L CH_3OH electrolyte, taking Pt/C-JM as the benchmark. The mass activity curves are normalized by the actual Pt mass percentage (Table S1 in Supporting information) and shown in Fig. 2a. Clearly, there are two scan peaks, indicating that all catalysts exhibit a typical MOR feature. Specifically, the forward (I_f) and backward peak (I_b) corresponds to the oxidation of the methanol molecules and reaction intermediates, respectively [36]. Pt-Co-P/NPC exhibits a much better mass activity of 1016 mA/mg_{Pt}, remarkably outperforming Pt-P/Co_2P@NPC (345 mA/mg_{Pt}), Pt-P/NPC (617 mA/mg_{Pt}) and Pt/C-JM (640 mA/mg_{Pt}) (Fig. 2b). Moreover, this activity is also comparable to the state-of-the-art catalysts (Table S2 in Supporting information) reported in literatures. Of note, the support (Co_2P@NPC) is inactive for MOR (Fig. S10 in Supporting information). The comparison of MOR performances manifest that the promoting effect of Co_2P in MOR should originate from the resultant Pt-Co-P composite rather than Co_2P itself or the formed Pt-P composite.

In order to understand the remarkable advantages of Pt-Co-P/NPC over the other catalysts, their electrochemical active surface area (ECSA) values were firstly evaluated by CV in 0.5 mol/L H_2SO_4 electrolyte. As shown in Fig. 2c, the ECSA value of Pt-Co-P/NPC (41.3 m^2/g_{Pt}) is nearly twice that of Pt-P/Co_2P@NPC (21.6 m^2/g_{Pt}). This should be ascribed as the fact that the former has a smaller average particle size (Fig. S11 and Table S3 in Supporting information) [37]. Accordingly, the resultant Pt-Co-P/NPC has the advantages in downsizing the particle size and thus increasing the ECSA value in comparison to Pt-P/Co_2P@NPC. As a result, Pt-Co-P/NPC enables a larger number of active sites readily accessible to the reactants, partially responsible for its higher mass activity than that of Pt-P/Co_2P@NPC [12]. Besides, Pt-P/NPC and Pt/C-JM exhibit an ECSA of 47.2 and 44.9 m^2/g_{Pt}, respectively. These values are comparable to that of Pt-Co-P/NPC, even though the particle size of Pt/C-JM is remarkably larger than the other two catalysts. This may be because the surfaces of particles in Pt-Co-P/NPC and Pt-P/NPC are not completely comprised of Pt atoms [38].

The specific activity is a good indictor to characterize the intrinsic activity of MOR catalysts [5]. As shown in Figs. 2d and e, Pt-Co-P/NPC possesses a specific activity of 2.58 mA/cm^2, which is significantly higher than those of Pt-P/Co_2P@NPC (1.60 mA/cm^2), Pt-P/NPC (1.25 mA/cm^2) and Pt/C-JM (1.43 mA/cm^2). Thus, Pt-Co-P/NPC composite possesses the highest intrinsic activity to catalyze MOR. An electrochemical impedance spectroscopy (EIS) analysis was further applied to explore the electrode kinetics in the MOR process. The results are shown in Fig. 2f, and the fitting data are presented in Table S4 (Supporting information). Clearly, Pt-Co-P/NPC exhibits the lowest charge transfer resistance (R_{ct}) value in the Nyquist plots, further confirming its highest catalytic activity [23,39].

To understand the high activity of Pt-Co-P composite for MOR, the surface environment and valence states of the synthesized catalysts and the Pt/C-JM were delicately investigated by XPS. As shown in Fig. 3a, the Co 2p spectrum of Pt-Co-P/NPC can be well fitted to Co^{3+} (780.7 and 796.3 eV), Co^{2+} (782.7 and 798.6 eV) and satellite peaks (787.6 and 803.1 eV) [5,27]. Analogous features can be also seen in Pt-P/Co_2P@NPC, but these characteristic peaks in Pt-Co-P/NPC exhibits an obvious positive shift. P 2p spectra of Pt-Co-P/NPC, Pt-P/Co_2P@NPC and Pt-P/NPC (Fig. 3b) are quite similar. All can be classified as the P-O and P-C characteristics [35,40]. Of note, the binding energy of P 2p in Pt-Co-P/NPC delivers a positive shift than that in Pt-P/Co_2P@NPC and Pt-P/NPC. The above results suggest that the formation of Pt-Co-P composite may enhance electron depletion of Co and P atoms [13,34].

The Pt 4f spectra of the four catalysts are given in Fig. 3c. Clearly, Pt-Co-P/NPC exhibits characteristic peaks that can be well attributed to Pt^0 (71.21 and 74.60 eV) and Pt^{2+} (72.40 and 75.85 eV) [15]. The binding energy of Pt 4f in Pt-Co-P/NPC exhibits an evident down shift of 0.6 eV in comparison to that of Pt/C-JM. The shift is more remarkable than that of Pt-P/Co_2P@NPC and Pt-P/NPC. In light of the above-mentioned variations of Co 2p and P 2p states, the formation of Pt-Co-P composite enhances electron transfer from Co and P to Pt and thus results in electron-rich Pt centers. This is also supported by our theoretical calculations (Fig. S13 in Supporting information). The calculated charge density difference of embedding a P or a Co atom in the surface of Pt (111) reveal that charge transfers from P or Co to Pt atoms. These results clearly indicate a significantly stronger electronic effect between Co, P and Pt in Pt-Co-P/NPC composite catalyst than in Pt-P/Co_2P@NPC. The down-shift of Pt 4f binding energy in Pt-Co-P/NPC suggests a lower D-band center, which is expected to result in a weaker CO adsorption on Pt sites [41]. Accordingly, Pt-Co-P/NPC may enable a higher CO tolerance and thus a higher intrinsic activity for MOR [5], partially contributing to its higher mass activity than that of Pt-P/Co_2P@NPC.

To gain deep insight into the superior MOR performance upon the formation of Pt-Co-P composite, we performed comparative DFT calculations about two crucial descriptors for MOR, *i.e.*, water dissociation and CO adsorption on modeled Pt (111), Pt-P (111) and Pt-Co-P (111) surfaces [42,43]. As shown in Fig. 3d, the calculated free energy of water dissociation on Pt (111) is positive. The endothermic nature reflects a sluggish kinetics, consistent with previous studies [44]. Upon introduction of P, the process becomes exothermic, indicating a faster reaction rate. Specifically, the reaction is even more exothermic when Pt-Co-P com-

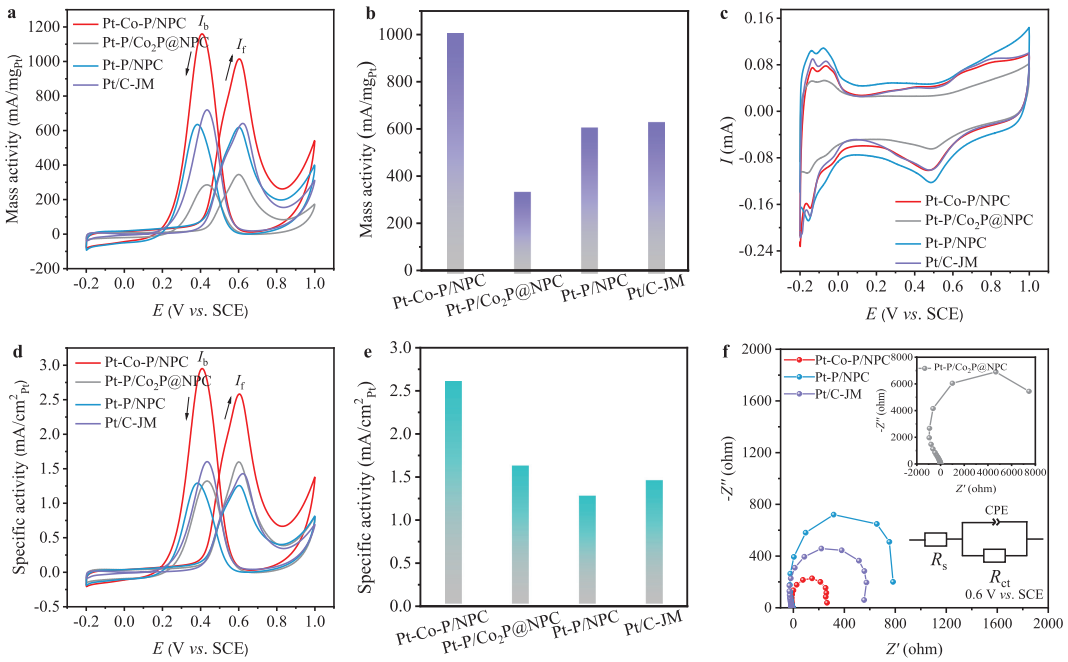

Fig. 2. (a, d) CV curves, (b) mass activity and (e) specific activity values of Pt-Co-P/NPC, Pt-P/Co_2P@NPC, Pt-P/NPC and Pt/C-JM in 0.5 mol/L H_2SO_4 + 1 mol/L CH_3OH electrolyte. (c) CV curves of the catalysts in 0.5 mol/L H_2SO_4 electrolyte. (f) The Nyquist plots of the above catalysts in 0.5 mol/L H_2SO_4 + 1 mol/L CH_3OH electrolyte. The inset in (f) is the relevant equivalent circuit.

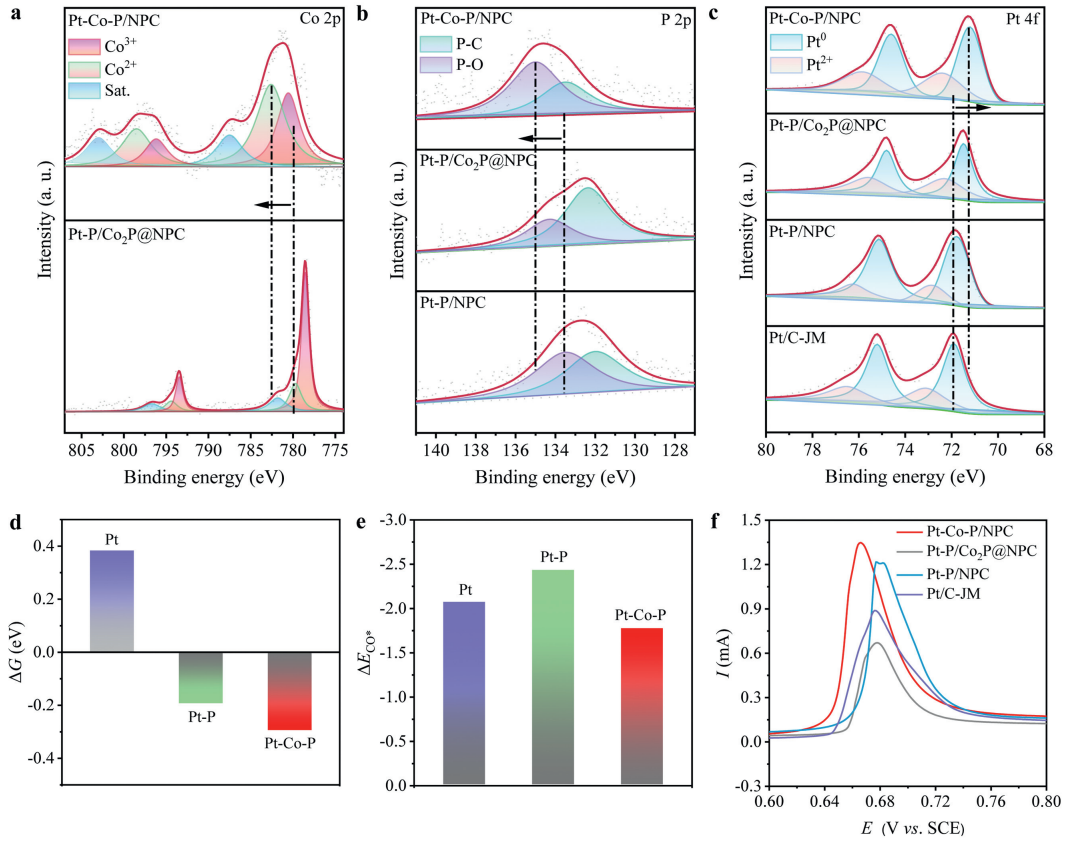

Fig. 3. XPS spectra of (a) Co 2p in Pt-Co-P/NPC and Pt-P/Co_2P@NPC, (b) P 2p in Pt-Co-P/NPC, Pt-P/Co_2P@NPC and Pt-P/NPC, (c) Pt 4f in Pt-Co-P/NPC, Pt-P/Co_2P@NPC, Pt-P/NPC and Pt/C-JM. (d) The reaction free energies of water dissociation. (e) CO adsorption energy on the three modeled surfaces. (f) CO stripping voltammetry curves of the catalysts in 0.5 mol/L H_2SO_4 electrolyte.

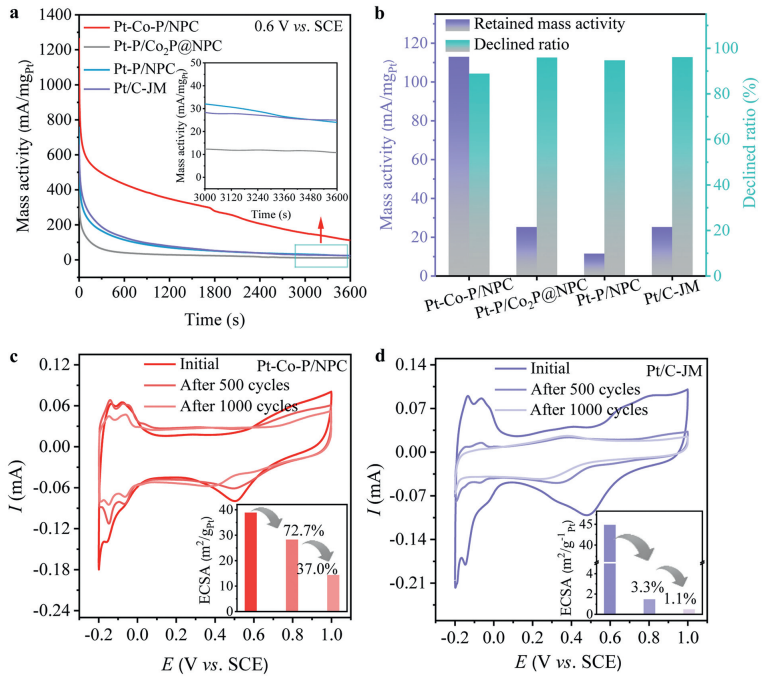

Fig. 4. (a) CA curves of Pt-Co-P/NPC, Pt-P/Co_2P@NPC, Pt-P/NPC and Pt/C-JM in 0.5 mol/L H_2SO_4 + 1 mol/L CH_3OH electrolyte. Inset shows the magnified image of the marked region. (b) The retained mass activity and activity declined ratio of the catalysts after CA test. The ADT curves of (c) Pt-Co-P/NPC and (d) Pt/C-JM in 0.5 mol/L H_2SO_4 electrolyte. Insets show the corresponding ECSA variations after ADT cycles.

posite is formed. According to the well-known Brønsted-Evans-Polanyi relations [45], the more negative reaction energy means the lower water dissociation barrier. Thus, water would dissociate most readily into H* and OH* on Pt-Co-P (111). The remarkably promoted OH* production on Pt-Co-P (111) would facilitate the removal of adsorbed CO* through a bi-functional mechanism ($CO^* + OH^* = CO_2 + H^*$) [25,46]. As for CO adsorption, it is clear that Pt-Co-P (111) exhibits the weakest strength towards CO* adsorption (Fig. 3e).

The above calculated results clearly indicate the formation of Pt-Co-P (111) surface would promote the removal of tightly bonded CO* from the surface and alleviate the well-known poisoning effect of CO [42]. These results are consistent with the CO stripping experiment, which is regarded as a convincing technique to evaluate CO tolerance in MOR [4,47]. As shown in Fig. 3f, the Pt-Co-P/NPC presents an obviously lower onset and peak potential (0.632 and 0.666 V) than Pt-P/Co_2P@NPC (0.640 and 0.676 V), Pt-P/NPC (0.649 and 0.680 V) and Pt/C-JM (0.658 and 0.690 V). The experimentally observed superior activity of Pt-Co-P/NPC towards MOR should originate largely from a high intrinsic activity for CO removal [5,48]. Moreover, theoretical calculations indicate that water energetically prefers adsorption on Co site (Fig. S14 in Supporting information) while CO adsorption on Pt sites is energetically more favorable. In combination with the strong electronic effect between Co, P and Pt in Pt-Co-P/NPC, the precise role of Pt-Co-P becomes clear. The presence of P and Co would result in electron-rich Pt centers and promotes water dissociation. Particularly, the Pt and Co sites may work in concert to properly address CO oxidation and thus synergistically act as active sites to accelerate MOR.

Apart from the catalytic activity, long-term stability of catalysts is equally important to the commercial application of DMFCs [4]. As is well-known, the MOR catalysts' stability is influenced by both chemical and physical factors. The former refers to the CO poisoning, degrading the catalytic activity promptly [48]. The latter is the structure damage during MOR, such as the dissolution, migration, ripening of Pt nanoparticles as well as support corrosion and collapse [49,50].

In this study, the chemical factor was evaluated by chronoamperometry (CA) at a fixed potential of 0.6 V. As shown in Fig. 4a, the mass activity decreases rapidly at the initial stage (< 1000s) due to the quick methanol consumption and CO poisoning near the electrode [14]. As the reaction proceeds, the methanol concentration tends to be constant, meanwhile, the production and consumption of CO reaches a dynamic equilibrium. As a result, the CA curves gradually flatten out. After 3600 s, Pt-Co-P/NPC possesses the lowest declined ratio (Fig. 4b), reflecting its best stability on account of its enhanced CO tolerance [5,51].

As for the physical factors, the accelerated durability test (ADT) of Pt-Co-P/NPC and Pt/C-JM were operated (Figs. 4c and d). The areas of the hydrogen desorption region decrease with the increase of ADT cycles, signifying the gradual destruction of both catalysts [49,50]. The ECSA of Pt/C-JM catalyst is decayed rapidly, and only 3.3% and 1.1% are maintained after 500 and 1000 cycles, respectively. In comparison, the Pt-Co-P/NPC has correspondingly 72.7% and 37.0% of ECSA values retained (the insets in Figs. 4c and d). Fig. S15 (Supporting information) shows the TEM images of Pt-Co-P/NPC and Pt/C-JM after ADT for 1000 cycles. Pt nanoparticles in Pt/C-JM suffer from serious agglomeration and are unevenly dispersed. In contrast, the dispersion of Pt-Co-P nanoparticles remains uniform though inevitable particle agglomeration still occurs. Therefore, Pt-Co-P/NPC possesses better structure stability, explaining its higher retained ECSA values.

Our controlled experiments demonstrate that the resultant Pt-Co-P composite is the real active species when Co_2P is applied as the co-catalysts for MOR. The advantages of Pt-Co-P in catalyzing MOR can be ascribed as the following aspects: (i) The *in-situ* formed Pt-Co-P enables a larger ECSA value and thus more exposed active sites accessible for reactants. (ii) The enhanced electron interaction in Pt-Co-P weakens the chemisorption strength of CO* and promotes water dissociation into OH*. Accordingly, the Pt-Co-

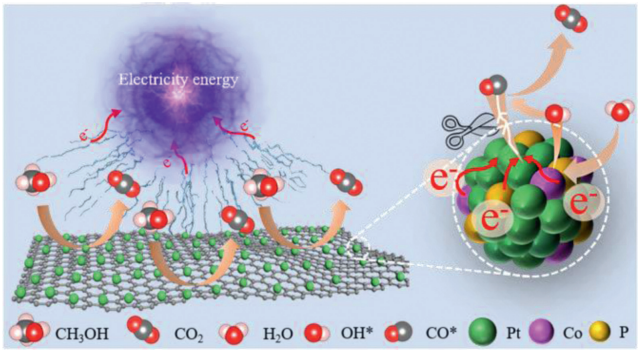

Scheme 2. Schematic illustration of the catalytic mechanism for MOR of Pt-Co-P/NPC.

P composite could facilitate the removal of adsorbed CO* through a bi-functional mechanism (Scheme 2) and ultimately accelerate MOR. Our study not only presents an effort to identify the real promoting species and mechanisms of TMPs in MOR, but also makes an essential step in development of high-performance TMPs-based MOR catalysts. Such mechanistic understanding is undoubtedly of significance for the development of advanced TMPs-based MOR catalysts and ultimately the wide penetration of DMFCs devices.

In summary, to probe the real promoting effects of TMPs-based MOR catalysts, we conducted a series of controlled experiments to preserve or etch Co_2P respectively using K_2PtCl_6 and H_2PtCl_6 as Pt sources during deposition process. Co_2P is well-preserved and totally transformed into Pt-Co-P in the former and latter cases, respectively. Our results demonstrate that the promoting effect of Co_2P is ascribed primarily to the resultant Pt-Co-P composite rather than Co_2P itself. This is in sharp contrast to previous reports, which claimed that TMPs themselves play the dominant role in enhancing MOR performance. Mechanistic analysis reveals that Pt-Co-P/NPC exhibits better CO tolerance than Pt-P@Co_2P/NPC, Pt-P/NPC and Pt/C-JM due to its weaker CO* adsorption strength and higher OH* supply capacity. This work sheds a new light on the promoting effects of TMPs-based MOR catalysts, which will stimulate the exploration of advanced MOR catalysts.

Declaration of competing interest

The authors declare that they have no known competing financial interests or personal relationships that could have appeared to influence the work reported in this paper.

Acknowledgments

This work was financially supported from the National Natural Science Foundation of China (Nos. 12074048 and 12147102), the Project for Fundamental and Frontier Research in Chongqing (No. cstc2020jcyj-msxmX0796), and the Fundamental Research Funds for the Central Universities (No. 2022CDJXY-002). We would like to thank Prof. Danmei Yu for her helpful experimental details.

Supplementary materials

Supplementary material associated with this article can be found, in the online version, at doi:10.1016/j.cclet.2022.107899.

References

[1] S. Zhang, Z. Zeng, Q. Li, et al., Energy Environ. Sci. 14 (2021) 5911–5918.
[2] L. Huang, X. Zhang, Q. Wang, et al., J. Am. Chem. Soc. 140 (2018) 1142–1147.
[3] C. Zhang, L. Xu, J. Chen, Chin. Chem. Lett. 27 (2016) 832–836.
[4] W. Huang, H. Wang, J. Zhou, et al., Nat. Commun. 6 (2015) 10035–10042.
[5] J. Ding, W. Hu, L. Ma, et al., J. Power Sources 481 (2021) 228888.
[6] M. Jiang, Y. Hu, W. Zhang, et al., Chem. Mater. 33 (2021) 3767–3778.
[7] X. Wu, J. Zhao, Y. Wu, et al., ACS Appl. Mater. Interfaces. 10 (2018) 12740–12749.
[8] L. Hui, X. Zhang, Y. Xue, et al., J. Am. Chem. Soc. 144 (2022) 1924–1928.
[9] B. Fang, Z. Liu, Y. Bao, L. Feng, Chin. Chem. Lett. 31 (2020) 2259–2262.
[10] Y. Zhao, J. Liu, C. Liu, F. Wang, Y. Song, ACS Catal. 6 (2016) 4127–4134.
[11] M. Jiang, L. Ma, M. Gan, et al., Electrochim. Acta 293 (2019) 30–39.
[12] H. Li, Q. Fu, L. Xu, et al., Energy Environ. Sci. 10 (2017) 1751–1756.
[13] G. Zhang, Z. Yang, W. Zhang, Y. Wang, J. Mater. Chem. A 5 (2017) 1481–1487.
[14] M. Huang, J. Zhang, C. Wu, L. Guan, ACS Appl. Mater. Interfaces 9 (2017) 26921–26927.
[15] F. Xie, L. Ma, M. Gan, et al., J. Power Sources 420 (2019) 73–81.
[16] Z. Yan, G. He, P. Shen, et al., J. Mater. Chem. A 2 (2014) 4014–4022.
[17] C. He, P. Shen, Nano Energy 8 (2014) 52–61.
[18] F. Yu, Y. Xie, H. Tang, et al., Electrochim. Acta 264 (2018) 216–224.
[19] J. Zhang, L. Ma, M. Gan, S. Fu, Y. Zhao, J. Power Sources 324 (2016) 199–207.
[20] J. Chang, L. Feng, C. Liu, W. Xing, X. Hu, Energy Environ. Sci. 7 (2014) 1628–1632.
[21] Z. Xing, Q. Liu, A. Asiri, X. Sun, Adv. Mater. 26 (2014) 5702–5707.
[22] J. Chang, L. Feng, K. Jiang, et al., J. Mater. Chem. A 4 (2016) 18607–18613.
[23] L. Feng, K. Li, J. Chang, C. Liu, W. Xing, Nano Energy 15 (2015) 462–469.
[24] D. Wei, L. Ma, M. Gan, et al., Int. J. Hydrog. Energy 45 (2020) 4875–4886.
[25] A. Nassr, I. Sinev, M. Pohl, W. Grünert, M. Bron, ACS Catal. 4 (2014) 2449–2462.
[26] L. Feng, J. Chang, K. Jiang, et al., Nano Energy 30 (2016) 355–361.
[27] D. Das, K. Nanda, Nano Energy 30 (2016) 303–311.
[28] Y. Pan, K. Sun, S. Liu, et al., J. Am. Chem. Soc. 140 (2018) 2610–2618.
[29] J. Ma, B. Liu, R. Wang, et al., Chin. Chem. Lett. 33 (2022) 2585–2589.
[30] B. Xia, Y. Yan, N. Li, et al., Nat. Energy 1 (2016) 15006–15011.
[31] I. Amiinu, X. Liu, Z. Pu, et al., Adv. Fun. Mater. 28 (2018) 1704638–1704646.
[32] L. Jiao, W. Yang, G. Wan, et al., Angew. Chem. Int. Ed. 59 (2020) 20589–20595.
[33] H. Huang, S. Yang, R. Vajtai, X. Wang, P. Ajayan, Adv. Mater. 26 (2014) 5160–5165.
[34] L. Ding, A. Wang, G. Li, et al., J. Am. Chem. Soc. 134 (2012) 5730–5733.
[35] Z. Lu, J. Xie, J. Hu, K. Wang, Y. Cao, Small 17 (2021) 2104656–2104674.
[36] Y. Xie, H. Zhang, G. Yao, et al., J. Energy Chem. 26 (2017) 193–199.
[37] J. Ding, L. Ma, M. Gan, et al., Int. J. Hydrog. Energy 44 (2019) 30388–30400.
[38] H. Lv, D. Xu, L. Sun, et al., ACS Nano 13 (2019) 12052–12061.
[39] Y. Xu, S. Hou, G. Yang, et al., Electrochim. Acta 285 (2018) 192–201.
[40] S. Yang, M. Xie, L. Chen, et al., Int. J. Hydrog. Energy 44 (2019) 4543–4552.
[41] M. Thotiyl, T. Ravikumar, S. Sampath, J. Mater. Chem. A 20 (2010) 10643–10651.
[42] T. He, W. Wang, F. Shi, et al., Nature 598 (2021) 76–81.
[43] Q. Feng, S. Zhao, D. He, et al., J. Am. Chem. Soc. 140 (2018) 2773–2776.
[44] Z. Chen, G. Cao, L. Gan, et al., ACS Catal. 8 (2018) 8866–8872.
[45] L. Gan, R. Tian, X. Yang, H. Lu, Y. Zhao, J. Phys. Chem. C 116 (2011) 745–752.
[46] P. Ferrin, M. Manos, J. Am. Chem. Soc. 131 (2009) 14381–14389.
[47] X. Zhu, Z. Hu, M. Huang, et al., Chin. Chem. Lett. 32 (2021) 2033–2037.
[48] Y. Wang, C. Du, Y. Sun, et al., Electrochim. Acta 254 (2017) 36–43.
[49] H. Gasteiger, S. Kocha, B. Sompalli, F. Wagner, Appl. Catal. B: Environ. 56 (2005) 9–35.
[50] J. Wang, G. Yin, Y. Shao, et al., J. Power Sources 171 (2007) 331–339.
[51] H. Qiu, X. Dong, B. Sana, et al., ACS Appl. Mater. Interfaces 5 (2013) 782–787.